Sliding coherence window technique for hierarchical detection
of continuous gravitational waves

Holger J. Pletsch[*]

Max-Planck-Institut für Gravitationsphysik (Albert-Einstein-Institut) and Leibniz Universität Hannover,
Callinstraße 38, D-30167 Hannover, Germany
(Received 7 February 2011; published 3 June 2011)

A novel hierarchical search technique is presented for all-sky surveys for continuous gravitational-wave sources, such as rapidly spinning nonaxisymmetric neutron stars. Analyzing yearlong detector data sets over realistic ranges of parameter space using fully coherent matched-filtering is computationally prohibitive. Thus more efficient, so-called hierarchical techniques are essential. Traditionally, the standard hierarchical approach consists of dividing the data into nonoverlapping segments of which each is coherently analyzed, and subsequently the matched-filter outputs from all segments are combined incoherently. The present work proposes to break the data into subsegments shorter than the desired maximum coherence time span (size of the coherence window). Then matched-filter outputs from the different subsegments are efficiently combined by sliding the coherence window in time: Subsegments whose timestamps are closer than coherence window size are combined coherently, otherwise incoherently. Compared to the standard scheme at the same coherence time baseline, data sets longer by about 50–100% would have to be analyzed to achieve the same search sensitivity as with the sliding coherence window approach. Numerical simulations attest to the analytically estimated improvement.

I. INTRODUCTION

Rapidly rotating neutron stars are anticipated to emit continuous gravitational-wave (CW) signals through various plausible scenarios [1–6] due to asymmetries. While the majority of such neutron stars eludes electromagnetic observations, their population might potentially be probed only by means of gravitational waves [7]. Currently, an international network of laser-interferometric detectors [8–11] is in operation. The observational upper limits obtained from known radio pulsars [12,13] and all-sky surveys [14–18] already constrain the physics of neutron stars, and thus a detection of a CW signal from a spinning neutron star would shed light on their currently rather uncertain physics [19].

Extremely sensitive data analysis techniques are needed to detect prior unknown CW sources because of their expected low signal-to-noise ratios. A powerful method has been derived [20] based on the principle of maximum likelihood detection, leading to coherent matched filtering. CW signals are quasimonochromatic with a slowly changing intrinsic frequency. However, the Earth's motion relative to the solar system barycenter (SSB) generates a Doppler modulation in amplitude and phase of the waveform at a terrestrial detector. As shown in [20], the coherent matched-filtering statistic can be analytically maximized over the *amplitude parameters* describing the signal's amplitude variation. The so-obtained coherent detection statistic is referred to as the $\mathcal{F}$-statistic, which can also include multiple detector data streams [21]. Thus, an explicit search (evaluating $\mathcal{F}$) is only done over the *phase parameters* describing the signal's phase evolution: the source's sky location, frequency, and frequency derivatives ("spindowns").

However, what ultimately limits the search sensitivity in scanning the entire sky for previously unknown CW sources is the finite computational resources. For yearlong data sets, searching a realistic portion of parameter space is computationally absolutely impractical [20,22]. This is due to the apparently enormous number of template waveforms needed to discretely cover the search parameter space, increasing as a high power of the coherent integration time. In consequence, viable all-sky fully coherent $\mathcal{F}$-statistic searches are restricted to much shorter coherent integration times, despite that the $\mathcal{F}$-statistic can be very efficiently computed using the fast Fourier transform (FFT) algorithm [20,23].

All-sky surveys sifting through yearlong data sets for previously unknown isolated CW sources are accomplished by incoherently combining either excess power or $\mathcal{F}$-statistic values from shorter segments of data. In the power-combining methods [14,15], the segment duration is chosen short enough (typically, 30 minutes) so that the CW signal power resides in a single frequency bin during each segment. In contrast, so-called "hierarchical" $\mathcal{F}$-statistic-based methods [24–26] coherently track the CW signal phase over longer segments (typically of the order of a day or a few days).

In this work, the "standard" hierarchical detection scheme refers to the following approach. Divide the data into nonoverlapping segments of duration T. Then, for a given point in search parameter space, the $\mathcal{F}$-statistic is

─────────────
[*]Holger.Pletsch@aei.mpg.de

computed separately for each segment, and subsequently $\mathcal{F}$ values from all segments are summed. Thus T defines the maximum time span of maintained phase coherence to the signal. This approach is efficient, because computing the coherent matched-filtering statistic $\mathcal{F}$ just over T allows one to use a *coarse* grid of templates in phase parameter space, compared to one required for the entire data set. Only when incoherently combining the $\mathcal{F}$-statistic results from all segments is a common *fine* grid of templates necessary.

Recent progress in understanding the global correlations [27,28] of the $\mathcal{F}$-statistic in the phase parameters has lead to a substantially more sensitive hierarchical search technique [26]. This method has addressed a long-standing problem, namely, the design of, and link between, the coarse and fine grids. A very useful geometric tool in this context is the concept of a metric, as first investigated in [29,30], measuring the fractional loss in expected $\mathcal{F}$-statistic for a given signal at a nearby grid point. While such a metric has been well studied for the coherent stage [22,31,32], in [26] the first analytical metric for the incoherent combination step has been found by exploiting new coordinates on the phase parameter space. This analytical "semicoherent metric" has lately been further studied and extended to greater generality in [33]. This technology is currently also implemented and employed by EINSTEIN@HOME [18], a volunteer distributed computing project carrying out the most sensitive all-sky CW surveys.

The present work presents a novel hierarchical search strategy which builds on the results of [26,33], while further enhancing the search sensitivity. Previous hierarchical search methods divide the data into nonoverlapping segments whose length is equal to coherent time baseline T. Here, a partitioning of the data into segments *shorter* than the desired maximum coherence length T is considered, and subsequently one "slides" a coherence window of size T over the segments. As a result, segments which are closer than coherence window size T are coherently combined and otherwise incoherently. This scheme also ensures that the same semicoherent metric as derived in [26,33] governs the template grid construction in phase parameter space but considerably enhances the overall search sensitivity.

Section II briefly recaps the continuous gravitational-wave signal waveform. Section III describes the coherent matched-filtering statistic $\mathcal{F}$ and what we refer to as the "standard hierarchical search scheme." The idea behind the sliding coherence window approach is elucidated in Sec. IV, along with an analytical sensitivity estimation. The improved performance is demonstrated in Sec. V by means of Monte Carlo simulations. In addition, Sec. VI compares the estimated sensitivity at fixed computational cost. Finally, concluding remarks follow in Sec. VII.

II. CONTINUOUS GRAVITATIONAL-WAVE SIGNALS

The dimensionless signal response function $h(t)$ of an interferometric detector to a weak plane gravitational wave in the long-wavelength approximation is a linear combination of the form [20],

$$h(t) = F_+(t)h_+(t) + F_\times(t)h_\times(t). \tag{1}$$

The antenna pattern functions $F_+(t)$ and $F_\times(t)$ are given by

$$F_+(t) = a(t)\cos 2\psi + b(t)\sin 2\psi, \tag{2a}$$
$$F_\times(t) = b(t)\cos 2\psi - a(t)\sin 2\psi, \tag{2b}$$

where ψ represents the polarization angle of the signal, and the angle between the detector arms is assumed to be $\pi/2$. For explicit expressions of the functions $a(t)$ and $b(t)$, the reader is referred to Ref. [20].

In the case of an isolated, rapidly rotating neutron star with a nonaxisymmetric deformation and negligible proper motion (cf. [34,35]), the waveforms corresponding to the plus $(+)$ and cross $(\times)$ polarizations are

$$h_+(t) = A_+\sin\Psi(t), \qquad h_\times(t) = A_\times\cos\Psi(t), \tag{3}$$

where A_+ and $A_\times$ are the constant plus and cross polarization amplitude parameters, respectively, and $\Psi(t)$ is the phase of the signal. The parameters A_+ and $A_\times$ can be expressed in terms of the gravitational-wave strain tensor amplitude h_0 and the inclination angle ι as

$$A_+ = h_0(1 + \cos^2\iota)/2, \qquad A_\times = h_0\cos\iota. \tag{4}$$

The phase $\Psi(t)$ of the CW signal at detector time t takes the following form [20]:

$$\begin{aligned}\Psi(t) &= \Phi_0 + \Phi(t) \\ &= \Phi_0 + 2\pi\sum_{k=0}^{s}\frac{f^{(k)}(t_0)}{(k+1)!}\left[t - t_0 + \frac{\vec{r}(t)\cdot\vec{n}}{c}\right]^{k+1},\end{aligned} \tag{5}$$

where Φ_0 is the initial phase, $f^{(0)} \equiv f$ denotes the frequency, and $f^{(k>0)}$ is the kth frequency time derivative (also called "spindown"), evaluated at the SSB at reference time t_0. The integer $s > 0$ denotes the number of frequency time derivatives to be taken into account; therefore, it holds $f^{(k>s)} = 0$. The vector $\vec{r}(t)$ connects from the SSB to the detector, c is the speed of light, and $\vec{n}$ is a constant unit vector pointing from the SSB to the location of the CW source. The source's sky location is determined by two independent coordinates, for example, one can use equatorial coordinates of right ascension and declination, denoted by α and δ, respectively. In these coordinates: $\vec{n} = (\cos\delta\cos\alpha, \cos\delta\sin\alpha, \sin\delta)$. The collection of phase parameters will be summarized by the vector $\mathbf{p} \equiv (f, f^{(1)}, \ldots, f^{(s)}, \alpha, \delta)$.

Using Eqs. (2), (3), and (5), it is possible to rewrite Eq. (1) as follows:

$$h(t) = \sum_{\mu=1}^{4} \mathcal{A}_\mu h_\mu(t), \qquad (6)$$

where the four amplitude parameters $(A_+, A_\times, \psi, \Phi_0)$ have been reparametrized by the 4-vector $\mathcal{A} \equiv (\mathcal{A}_1, \mathcal{A}_2, \mathcal{A}_3, \mathcal{A}_4)$, whose individual components are

$$\begin{aligned}
\mathcal{A}_1 &= A_+ \cos2\psi \cos\Phi_0 - A_\times \sin2\psi \sin\Phi_0, \\
\mathcal{A}_2 &= A_+ \sin2\psi \cos\Phi_0 + A_\times \cos2\psi \sin\Phi_0, \\
\mathcal{A}_3 &= -A_+ \cos2\psi \sin\Phi_0 - A_\times \sin2\psi \cos\Phi_0, \\
\mathcal{A}_4 &= -A_+ \sin2\psi \sin\Phi_0 + A_\times \cos2\psi \cos\Phi_0,
\end{aligned} \qquad (7)$$

and the functions $h_\mu(t)$ have been defined as

$$\begin{aligned}
h_1(t) &= a(t)\cos\Phi(t), & h_2(t) &= b(t)\cos\Phi(t), \\
h_3(t) &= a(t)\sin\Phi(t), & h_4(t) &= b(t)\sin\Phi(t).
\end{aligned} \qquad (8)$$

III. STANDARD HIERARCHICAL DETECTION SCHEME

At a given detector time t, the detector output data time series is denoted by $x(t)$. In the absence of any signal, the data contain only noise $n(t)$, which is assumed to be a zero-mean, stationary, and Gaussian random process [36]. When a signal $h(t)$ is present, the noise is assumed to be additive, so that $x(t) = n(t) + h(t)$.

For simplicity, in this work only a single-detector input data stream is considered. However, based on the results of [21] (and also [32]), it is straightforward to generalize the proposed search technique to multiple-detector input data, as well as to time-varying noise.

To contrast with the sliding coherence window approach, this section describes the standard hierarchical detection scheme which sums one $\mathcal{F}$-statistic value from each of N *nonoverlapping* segments of duration T. For simplicity, in this presentation the data set is taken to be contiguous, so that the total data time span is written as $T_{\text{data}} = NT$. The individual segments are labeled by the index $j = 1, \ldots, N$. Let t_j denote the time midpoint of segment j, which thus spans the time interval $[t_j - T/2, t_j + T/2]$.

A. Coherent matched-filtering of one segment

1. The $\mathcal{F}$-statistic

The likelihood ratio Λ_j for the jth segment, deciding between the hypothesis of a signal $h(t)$ with amplitude parameters $\mathcal{A}$ and phase parameters **p**, and no signal being present, is written as [20],

$$\ln\Lambda_j = (x|h)_j - \frac{1}{2}(h|h)_j, \qquad (9)$$

where the following inner product has been used [20],

$$(x|y)_j \equiv \frac{2}{S_n^{[j]}} \int_{t_j - T/2}^{t_j + T/2} x(t)y(t)dt, \qquad (10)$$

with $S_n^{[j]}$ defined as the one-sided noise spectral density for the jth segment. Since this work is concerned with narrow-bandwidth signals, $S_n^{[j]}$ is here taken as constant.

As was done in Ref. [20], the following inner products are combined for every segment j into a 4×4 matrix $\mathcal{M}^{[j]}$ whose components are

$$\mathcal{M}_{\mu\nu}^{[j]} \equiv (h_\mu|h_\nu)_j, \qquad (11)$$

where $\mu, \nu = 1, 2, 3, 4$. To very good accuracy, one can approximate [20],

$$(h_1|h_3)_j \approx (h_1|h_4)_j \approx (h_2|h_3)_j \approx (h_2|h_4)_j \approx 0, \quad (12a)$$

$$(h_1|h_1)_j \approx (h_3|h_3)_j \approx \frac{1}{2}A_j, \qquad (12b)$$

$$(h_2|h_2)_j \approx (h_4|h_4)_j \approx \frac{1}{2}B_j, \qquad (12c)$$

$$(h_1|h_2)_j \approx (h_3|h_4)_j \approx \frac{1}{2}C_j, \qquad (12d)$$

with the definitions

$$A_j \equiv (a|a)_j, \qquad B_j \equiv (b|b)_j, \qquad C_j \equiv (a|b)_j. \quad (13)$$

In addition, we abbreviate the linear correlations $(x|h_\mu)_j$ by the following compact notation:

$$x_\mu^{[j]} \equiv (x|h_\mu)_j. \qquad (14)$$

Thus, Eq. (9) is rewritten as

$$\ln\Lambda_j = \sum_{\mu=1}^{4} \mathcal{A}_\mu x_\mu^{[j]} - \frac{1}{2}\sum_{\mu,\nu=1}^{4} \mathcal{A}_\mu \mathcal{M}_{\mu\nu}^{[j]} \mathcal{A}_\nu. \qquad (15)$$

For every segment j the log-likelihood ratio of Eq. (15) is analytically maximized over the amplitude parameters $\mathcal{A}$. The maximum likelihood (ML) estimators for $\mathcal{A}$ obtained from the jth segment are denoted by

$$\hat{\mathcal{A}}^{[j]} = (\hat{\mathcal{A}}_1^{[j]}, \hat{\mathcal{A}}_2^{[j]}, \hat{\mathcal{A}}_3^{[j]}, \hat{\mathcal{A}}_4^{[j]}), \qquad (16)$$

are explicitly given by [20],

$$\begin{aligned}
\hat{\mathcal{A}}_1^{[j]} &= 2\frac{B_j x_1^{[j]} - C_j x_2^{[j]}}{D_j}, & \hat{\mathcal{A}}_2^{[j]} &= 2\frac{A_j x_2^{[j]} - C_j x_1^{[j]}}{D_j}, \\
\hat{\mathcal{A}}_3^{[j]} &= 2\frac{B_j x_3^{[j]} - C_j x_4^{[j]}}{D_j}, & \hat{\mathcal{A}}_4^{[j]} &= 2\frac{A_j x_4^{[j]} - C_j x_3^{[j]}}{D_j},
\end{aligned} \qquad (17)$$

where $D_j \equiv A_j B_j - C_j^2$, and $D_j \neq 0$ has been assumed.

Replacing the amplitude parameters $\mathcal{A}$ in $\ln\Lambda_j$ of Eq. (15) with their ML estimators $\hat{\mathcal{A}}^{[j]}$ given by Eqs. (17) yields the so-called $\mathcal{F}$-statistic for the jth segment,

$$\mathcal{F}_j \equiv \frac{B_j}{D_j}(x_1^{[j]^2} + x_3^{[j]^2}) + \frac{A_j}{D_j}(x_2^{[j]^2} + x_4^{[j]^2})$$
$$- \frac{2C_j}{D_j}(x_1^{[j]}x_2^{[j]} + x_3^{[j]}x_4^{[j]}). \qquad (18)$$

This expression can be written compactly by using the four-vector notation for the set of four linear correlations $x_\mu^{[j]}$ as

$$x^{[j]} \equiv (x_1^{[j]}, x_2^{[j]}, x_3^{[j]}, x_4^{[j]}), \qquad (19)$$

such that Eq. (18) takes the form

$$\mathcal{F}_j = \frac{1}{2}x^{[j]}\mathcal{M}^{[j]-1}x^{[j]^T}, \qquad (20)$$

where the superscript ^{T} indicates the transpose. Therefore, the $\mathcal{F}$-statistic represents a quadratic form in terms of the linear correlations $x_\mu^{[j]}$. It should be noted that in practice $\mathcal{F}_j$ can be efficiently computed using the FFT algorithm when rewriting the four linear correlations $x_\mu^{[j]}$ as two complex integrals; further details are described in [20,23].

We find that the $\mathcal{F}$-statistic can be equivalently formulated as a quadratic form in terms of the ML estimators $\hat{\mathcal{A}}_\mu^{[j]}$. Using Eqs. (17) to substitute the $x_\mu^{[j]}$ in Eq. (18) yields

$$\mathcal{F}_j = \frac{A_j}{4}(\hat{\mathcal{A}}_1^{[j]^2} + \hat{\mathcal{A}}_3^{[j]^2}) + \frac{B_j}{4}(\hat{\mathcal{A}}_2^{[j]^2} + \hat{\mathcal{A}}_4^{[j]^2})$$
$$+ \frac{C_j}{2}(\hat{\mathcal{A}}_1\hat{\mathcal{A}}_2 + \hat{\mathcal{A}}_3\hat{\mathcal{A}}_4), \qquad (21)$$

which is compactly rewritten as

$$\mathcal{F}_j = \frac{1}{2}\hat{\mathcal{A}}^{[j]}\mathcal{M}^{[j]}\hat{\mathcal{A}}^{[j]^T}, \qquad (22)$$

showing that the $\mathcal{F}$-statistic can also be viewed as quadratic form in terms of the $\hat{\mathcal{A}}_\mu^{[j]}$ with a coefficient matrix being equal to $\mathcal{M}^{[j]}$. This formulation (22) of the $\mathcal{F}$-statistic is not common in the existing literature, but closely related is the work of [38–40]. There, the matrix $\mathcal{M}^{[j]}$ is considered as a metric on the amplitude parameter space $\mathcal{A}$, and a norm of the four-vector $\mathcal{A}$ is defined by $\|\mathcal{A}\| \equiv \sqrt{\mathcal{A}\mathcal{M}^{[j]}\mathcal{A}^T}$. In this context, we see from Eq. (22) that the $\mathcal{F}$-statistic is simply half the squared "length" of the four-vector $\hat{\mathcal{A}}^{[j]}$ of amplitude ML estimators: $\mathcal{F}_j = \|\hat{\mathcal{A}}^{[j]}\|^2/2$.

2. Statistical properties

The four linear correlations $x_\mu^{[j]}$ for a given segment j are Gaussian distributed random variables, whose expectation values and variances, respectively, are in absence of a signal, when $x(t) = n(t)$, obtained as

$$E_n[x_\mu^{[j]}] = 0, \qquad E_n[x_\mu^{[j]}x_\nu^{[j]}] = \mathcal{M}_{\mu\nu}^{[j]}. \qquad (23)$$

Therefore, in this case, the probability density function of $2\mathcal{F}_j$ is a central χ^2 distribution with 4 degrees of freedom [20]. Hence, $2\mathcal{F}_j$ has the following expectation value and variance, respectively:

$$E_n[2\mathcal{F}_j] = 4, \qquad \sigma_{2\mathcal{F}_j,n}^2 = 8. \qquad (24)$$

When a signal is present, which perfectly matches the template waveform $h(t)$, then the expectation values corresponding to Eqs. (23) are obtained as

$$E_h[x_\mu^{[j]}] = (h|h_\mu)_j, \qquad (25)$$

$$E_h[x_\mu^{[j]}x_\nu^{[j]}] = \mathcal{M}_{\mu\nu}^{[j]} + (h|h_\mu)_j(h|h_\nu)_j. \qquad (26)$$

Thus, as first noted in [20], the covariance matrix for the Gaussian random variables $x_\mu^{[j]}$ is the *same* whether a signal is present or not, and it is exactly equal to $\mathcal{M}^{[j]}$. It should also be noted that the inverse of $\mathcal{M}^{[j]}$ is equal to the covariance matrix of the ML estimators $\hat{\mathcal{A}}_\mu^{[j]}$. Thus, in this case, $2\mathcal{F}_j$ has noncentral χ^2 distribution with 4 degrees of freedom and a noncentrality parameter $\rho_j^2 \equiv (h|h)_j$, where ρ_j is commonly referred to as the "optimal" signal-to-noise ratio (S/N). Thus, the expectation value and variance of $2\mathcal{F}_j$ in this perfect-match case are

$$E_h[2\mathcal{F}_j] = 4 + \rho_j^2, \qquad \sigma_{2\mathcal{F}_j,h}^2 = 8 + 4\rho_j^2, \qquad (27)$$

where ρ_j^2 is explicitly obtained as

$$\rho_j^2 = A_j\frac{\mathcal{A}_1^2 + \mathcal{A}_3^2}{2} + B_j\frac{\mathcal{A}_2^2 + \mathcal{A}_4^2}{2}$$
$$+ C_j(\mathcal{A}_1\mathcal{A}_2 + \mathcal{A}_3\mathcal{A}_4)$$
$$= \mathcal{A}\mathcal{M}^{[j]}\mathcal{A}^T, \qquad (28)$$

with $\mathcal{A}$ representing the 4-vector of the signal's amplitude parameters, $\mathcal{A} = (\mathcal{A}_1, \mathcal{A}_2, \mathcal{A}_3, \mathcal{A}_4)$. Comparing Eq. (28) to Eq. (22), we find that twice the $\mathcal{F}$-statistic can be interpreted as the ML estimator for the squared S/N: $2\mathcal{F}_j = \hat{\rho}_j^2$.

B. Incoherent combination of coherently analyzed segments

1. The standard hierarchical detection statistic

We denote the standard hierarchical detection statistic by $\bar{\mathcal{F}}$, which, as used in [24,26,33], represents the sum of one $\mathcal{F}$-statistic value $\mathcal{F}_j$ from each segment j,

$$\bar{\mathcal{F}} = \sum_{j=1}^{N} \mathcal{F}_j = \frac{1}{2}\sum_{j=1}^{N} x^{[j]}\mathcal{M}^{[j]-1}x^{[j]^T}, \qquad (29)$$

evaluated at a given fine-grid point in phase parameter space. Therefore, $\bar{\mathcal{F}}$ also represents a quadratic form in terms of the linear correlations $x_\mu^{[j]}$, and one can compactly rewrite Eq. (29) as

$$\bar{\mathcal{F}} = \frac{1}{2} x \bar{\mathcal{M}}^{-1} x^{\mathrm{T}}, \tag{30}$$

where the $4N$-vector x collects all the $x^{[j]}$ as

$$x = (x^{[1]}, x^{[2]}, \ldots, x^{[N]}), \tag{31}$$

and the $4N \times 4N$ matrix $\bar{\mathcal{M}}$ is defined to have the form

$$\bar{\mathcal{M}} = \begin{pmatrix} \mathcal{M}^{[1]} & & & \\ & \mathcal{M}^{[2]} & & \\ & & \ddots & \\ & & & \mathcal{M}^{[N]} \end{pmatrix}. \tag{32}$$

Hence, the standard hierarchical scheme, using the detection statistic $\bar{\mathcal{F}}$, represents the incoherent combination of *epochwise* coherent matched-filter outputs, where each epoch has duration T. Recall that, using Eq. (22), $\bar{\mathcal{F}}$ can equivalently be rewritten as a quadratic form in terms of the amplitude ML estimators $\hat{\mathcal{A}}^{[j]}$, leading to

$$\bar{\mathcal{F}} = \frac{1}{2} \sum_{j=1}^{N} \hat{\mathcal{A}}^{[j]} \mathcal{M}^{[j]} \hat{\mathcal{A}}^{[j]\mathrm{T}} = \frac{1}{2} \hat{\mathcal{A}} \bar{\mathcal{M}} \hat{\mathcal{A}}^{\mathrm{T}}, \tag{33}$$

where $\hat{\mathcal{A}}$ denotes the $4N$-vector $\hat{\mathcal{A}} = (\hat{\mathcal{A}}^{[1]}, \hat{\mathcal{A}}^{[2]}, \ldots, \hat{\mathcal{A}}^{[N]})$.

The problem of efficiently selecting the best coarse-grid $\mathcal{F}_j$ value in every segment for a given fine-grid point has been studied in previous work [26,33], and hence for rest of this paper it is assumed that such an efficient link between the coarse and fine grids is available.

2. Statistical properties

In absence of a signal, it is straightforward to show that the probability density function of $2\bar{\mathcal{F}}$ is a central χ^2 distribution with $4N$ degrees of freedom [24,35]; hence, $\bar{\mathcal{F}}$ has the expectation value and variance, respectively,

$$E_n[2\bar{\mathcal{F}}] = 4N, \qquad \sigma^2_{2\bar{\mathcal{F}},n} = 8N. \tag{34}$$

On the other hand, if a signal $h(t)$ is present, perfectly matching the template-waveform phase parameters, then $\bar{\mathcal{F}}$ has a noncentral χ^2 distribution with $4N$ degrees of freedom and noncentrality parameter $\bar{\rho}^2$. The expectation value and variance of $\bar{\mathcal{F}}$, respectively, are obtained as

$$E_h[2\bar{\mathcal{F}}] = 4N + \bar{\rho}^2, \qquad \sigma^2_{2\bar{\mathcal{F}},h} = 8N + 4\bar{\rho}^2, \tag{35}$$

where $\bar{\rho}$ is given by

$$\bar{\rho}^2 \equiv \sum_{j=1}^{N} \rho_j^2, \tag{36}$$

recalling that ρ_j as of Eq. (28) denotes the optimal S/N for the jth segment.

It is interesting to note that $\bar{\rho}$ of Eq. (36) is actually *equal* to the fully coherent optimal S/N for the entire data set. The apparent difference in search sensitivity results

from the different underlying probability distributions. In the standard hierarchical scheme, there are N times as many degrees of freedom as compared to the fully coherent case.

IV. SLIDING COHERENCE WINDOW APPROACH

The central idea behind the sliding coherence window scheme is to use a window the size of the coherence time baseline T and to "slide" it over the data set in steps *smaller* than T to combine the coherent matched-filter outputs from each sliding step. This effectively amounts to the incoherent combination of coherent matched-filter outputs from *overlapping* segments of length T, which remarkably improves the search sensitivity compared to the standard hierarchical scheme. There, only coherent matched-filter outputs from *nonoverlapping* segments of coherence length T are combined, omitting to coherently correlate large parts of the data which still lie *within* the coherence time baseline T, as illustrated in Fig. 1.
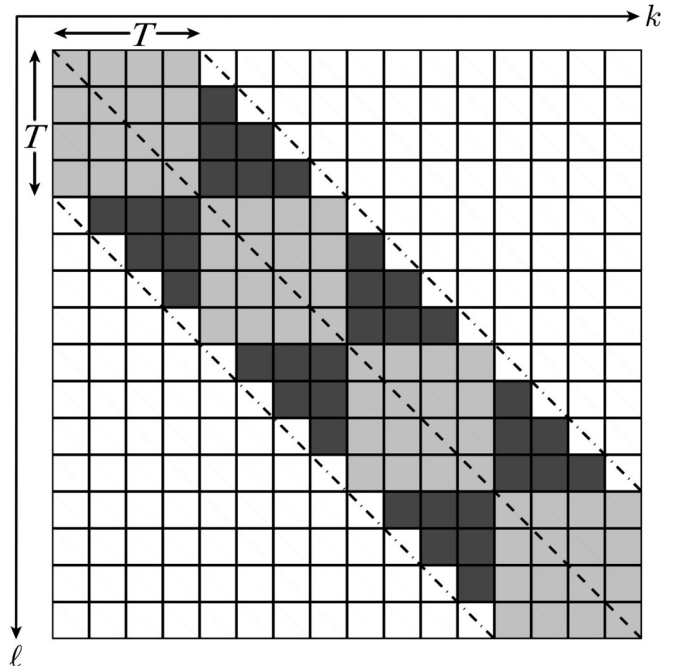

FIG. 1. Schematic comparison of the standard hierarchical search scheme and the sliding coherence window approach for the same coherence time baseline T. Each box represents one product of the linear correlations $x_\mu^{[k]} x_\mu^{[\ell]}$, obtained from the subsegments k and ℓ, respectively. In this example, the indices take the values $k, \ell = 1, \ldots, 16$. The light grey boxes represent the set of products selected in the standard hierarchical search scheme, for $N = 4$ coherent segments of duration T. The dark grey boxes are the products *additionally* selected by the sliding coherence window technique to enhance the search sensitivity. In this example, T is subdivided into $q = 4$ subsegments (implying a coherence overlap of $\eta = 75\%$ between successive sliding steps). In contrast, a fully coherent search over the entire data set would have to include all boxes shown.

The number of templates to discretely cover the phase parameter space searched is of great importance, since this is what ultimately limits the overall search sensitivity at the finite computing power available. Therefore, it should also be emphasized that the sliding coherence window technique employs the *same* number of templates in phase parameter space as the standard scheme. The combination of overlapping coherent integrations alters neither the coherence time baseline T nor the total data time span T_{data}. Hence, it is obvious that the same semicoherent metric as previously studied in [26,33] can also be used in combination with the here-proposed sliding coherence window technique [41].

A. Detection statistic

For computational efficiency, the sliding coherence window approach subdivides every data segment of duration T into q "subsegments," as adumbrated in Fig. 1. Hence, each subsegment is of duration $T_q = T/q$, which represents the step size between each sliding iteration of the coherence window.

The subsegments are labeled by $k = 1, \dots, qN$. Thus, in analogy to Eq. (19), we define the four-vector $x^{[k]}$ for the kth subsegment as $x^{[k]} = (x_1^{[k]}, x_2^{[k]}, x_3^{[k]}, x_4^{[k]})$. In this context, similarly to Eq. (31), the $4qN$-vector now collects all the $x^{[k]}$, $x = (x^{[1]}, x^{[2]}, \dots, x^{[qN]})$. Analogously, the same notation also applies to the $4qN$ amplitude ML estimators $\hat{\mathcal{A}}_\mu^{[k]}$.

As sketched in Fig. 1, the central goal of the sliding coherence window strategy is to combine a larger number of *distinct* pairs $\{x_\mu^{[k]}, x_\nu^{[\ell]}\}$ [44], while still restricting the maximum difference between their timestamps t_k and t_ℓ to at most the coherent time baseline T. Hence, the resulting selection condition is $|t_k - t_\ell| \leq T$.

To achieve this goal, in principle, an appropriate $4qN \times 4qN$ coefficient matrix $\mathcal{U}$ needs to be constructed, constituting the following quadratic form Z,

$$Z = \frac{1}{2} x \mathcal{U} x^{\text{T}}, \tag{37}$$

which represents the detection statistic of the sliding coherence window search technique.

In order to simplify the construction of $\mathcal{U}$, we exploit the fact that the constants C_k are typically much smaller than the values of A_k and B_k, and therefore terms involving C_k are neglected [45]. With this approximation, Eq. (37) should explicitly read as

$$Z = \sum_{k,\ell=1}^{qN} Q_T(t_k - t_\ell) \left[\frac{x_1^{[k]} x_1^{[\ell]} + x_3^{[k]} x_3^{[\ell]}}{\sqrt{A_k A_\ell}} \right. $$
$$\left. + \frac{x_2^{[k]} x_2^{[\ell]} + x_4^{[k]} x_4^{[\ell]}}{\sqrt{B_k B_\ell}} \right], \tag{38}$$

where the step function $Q_T(x)$ selects the pairs of linear correlations according to their time difference and the predefined coherent time baseline T,

$$Q_T(x) \equiv \begin{cases} 1 & |x| \leq T \\ 0 & |x| > T \end{cases}. \tag{39}$$

As with $\bar{\mathcal{F}}$, the detection statistic Z can also be equivalently reformulated as a quadratic form in terms of the amplitude ML estimators $\hat{\mathcal{A}}_\mu^{[k]}$. For practical convenience, in what follows we use $x_\mu^{[k]}$ as in Eq. (38). However, note that in the above approximative case, $x_\mu^{[k]} \propto \hat{\mathcal{A}}_\mu^{[k]}$, thus making the interchange between $x_\mu^{[k]}$ and $\hat{\mathcal{A}}_\mu^{[k]}$ simple if desired.

When $q = 1$, it is obvious that Z coincides with the standard hierarchical detection statistic $\bar{\mathcal{F}}$. However, if one chooses $q > 1$, the detection statistic Z is able to improve performance compared to $\bar{\mathcal{F}}$, as will be described in what follows.

Moreover, a useful quantity is denoted by η, which defines the average "coherence overlap" between successive sliding steps. For the case of a contiguous data set [46], as considered in this presentation, η is related to q simply via $\eta = 1 - 1/q$.

B. Statistical properties and sensitivity estimation

To analytically estimate the sensitivity of the sliding coherence window search, the underlying statistical properties are examined. Recall that, for simplicity, the data set has been taken as free of gaps, such that one can write the time span of the entire data set as $T_{\text{data}} = NT = qNT_q$. The detection statistic Z of Eq. (38) is explicitly written as

$$Z = \sum_{k=1}^{qN} \left\{ \frac{x_1^{[k]^2} + x_3^{[k]^2}}{A_k} + \frac{x_2^{[k]^2} + x_4^{[k]^2}}{B_k} \right.$$
$$\left. + 2 \sum_{\ell=k+1}^{k+q-1} \left[\frac{x_1^{[k]} x_1^{[\ell]} + x_3^{[k]} x_3^{[\ell]}}{\sqrt{A_k A_\ell}} + \frac{x_2^{[k]} x_2^{[\ell]} + x_4^{[k]} x_4^{[\ell]}}{\sqrt{B_k B_\ell}} \right] \right\}. \tag{40}$$

Since the actual probability density function of Z is cumbersome to work with, we approximate it here by a Gaussian distribution, which is well justified based on the generalized central limit theorem (provided $N \gg 1$), as done similarly in previous work [25]. Thus, we proceed by computing the mean and variance of Z.

When the data consist of zero-mean stationary Gaussian noise only, the expectation value of $2Z$ is obtained as

$$E_n[2Z] = 4qN, \tag{41}$$

and the variance of $2Z$ is given by

$$\sigma_{2Z,n}^2 = 8qN(2q - 1). \tag{42}$$

It is straightforward to show that for Gaussian noise, a certain false alarm probability P_{FA} corresponds to a threshold Z_{th} via

$$Z_{th} = E_n[Z] + \sigma_{Z,n}\sqrt{2}\,\text{erfc}^{-1}(2P_{FA}), \qquad (43)$$

where erfc denotes the complementary error function.

Provided the presence of a signal $h(t)$ whose phase parameters perfectly match the template, then the expectation value of $2Z$ is given by

$$E_h[2Z] = 4qN + \rho_Z^2, \qquad (44)$$

where we defined ρ_Z as

$$\rho_Z^2 \equiv \frac{\mathcal{A}_1^2 + \mathcal{A}_3^2}{2}\left\{\sum_{k=1}^{qN}\left[A_k + 2\sum_{\ell=k+1}^{k+q-1}\sqrt{A_k A_\ell}\right]\right\}$$
$$+ \frac{\mathcal{A}_2^2 + \mathcal{A}_4^2}{2}\left\{\sum_{k=1}^{qN}\left[B_k + 2\sum_{\ell=k+1}^{k+q-1}\sqrt{B_k B_\ell}\right]\right\}. \quad (45)$$

The probability of detection P_{DET} for Gaussian noise is given by

$$P_{DET} = \frac{1}{2}\,\text{erfc}\left(\frac{Z_{th} - E_h[Z]}{\sqrt{2}\sigma_{Z,h}}\right). \qquad (46)$$

For current ground-based detectors, the expected CW signals are extremely weak, so that the small-signal situation ($h \ll n$) is well justified. Thus, we approximate $\sigma_{Z,h}$ by using $\sigma_{Z,n}$ and, by means of Eqs. (42)–(45), one obtains from Eq. (46) the following relation:

$$\rho_Z^2 = \mathcal{E}\sqrt{2}\sigma_{Z,n}, \qquad (47)$$

where $\mathcal{E}$ has been defined as

$$\mathcal{E} \equiv \text{erfc}^{-1}(2P_{FA}) - \text{erfc}^{-1}(2P_{DET}). \qquad (48)$$

The minimum detectable gravitational-wave strain tensor amplitude h_0 can be determined from Eq. (47), because $h_0^2 \propto \rho_Z^2$ as follows from Eq. (45).

To obtain the estimated sensitivity scaling of the sliding coherence window search in terms of the most relevant parameters, the noise floor S_n is taken as constant throughout the data set. In addition, we replace the constants A_k and B_k by effective average values as $A_k \approx \frac{2T_q}{S_n}\bar{A}$, and $B_k \approx \frac{2T_q}{S_n}\bar{B}$, and define $\bar{\kappa}$ as

$$\bar{\kappa} \equiv \bar{A}(\bar{\mathcal{A}}_1^2 + \bar{\mathcal{A}}_3^2) + \bar{B}(\bar{\mathcal{A}}_2^2 + \bar{\mathcal{A}}_4^2), \qquad (49)$$

where the $\bar{\mathcal{A}}_\mu$ are the same as the $\mathcal{A}_\mu$ apart from the factor h_0, $\bar{\mathcal{A}}_\mu \equiv \mathcal{A}_\mu/h_0$. Thus, Eq. (45) simplifies to

$$\rho_Z^2 = h_0^2\bar{\kappa}\frac{T}{S_n}N(2q - 1). \qquad (50)$$

In turn, using Eq. (50) to substitute ρ_Z^2 in Eq. (47) and solving for h_0 yields

$$h_0 = \frac{2\sqrt{\mathcal{E}}}{\sqrt{\bar{\kappa}}}\sqrt{\frac{S_n}{T}}N^{-1/4}\left(2 - \frac{1}{q}\right)^{-1/4}, \qquad (51)$$

revealing the estimated sensitivity scaling of the sliding coherence window search. One may further rewrite Eq. (51) as

$$h_0 = \frac{2\sqrt{\mathcal{E}}}{\sqrt{\bar{\kappa}}}\sqrt{\frac{S_n}{T}}[N(1 + \eta)]^{-1/4}, \qquad (52)$$

using the previously introduced average coherence overlap η.

C. Comparison of sensitivity with standard scheme

Equation (52) also reveals the estimated sensitivity improvement of the sliding coherence window technique compared to the standard hierarchical search under the same assumptions. The standard hierarchical scheme is recovered for $\eta = 0$ (i.e., $q = 1$). Therefore, the sliding coherence window approach is more sensitive than the standard hierarchical search scheme by the factor $(1 + \eta)^{1/4}$. In terms of q, the sensitivity improvement factor is $(2 - 1/q)^{1/4}$, which is shown in Fig. 2.

The coherence overlap η enhances the search sensitivity effectively as if increasing the number of segments in the standard method. In other words, to achieve the same sensitivity as with the sliding coherence window technique at given T, using the standard hierarchical search method,
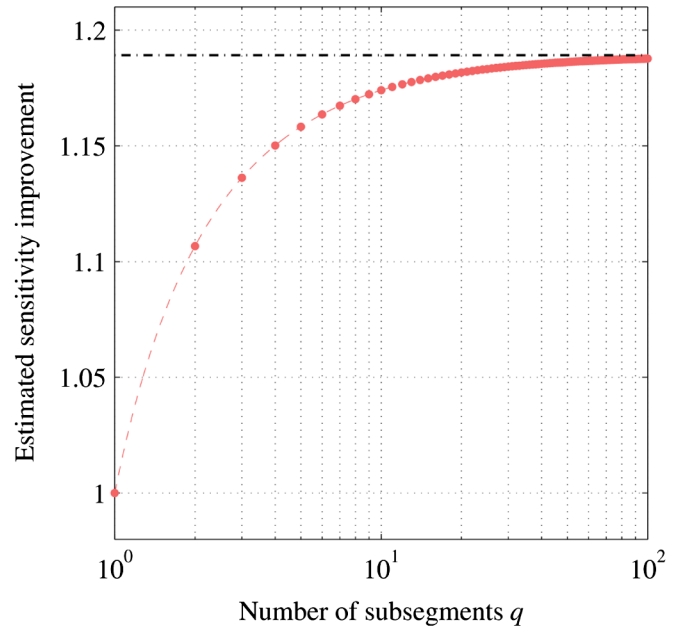

FIG. 2 (color online). Estimated sensitivity improvement factor of the sliding coherence window technique over the standard hierarchical search strategy, shown as a function of q (number of subsegments). The curve is explicitly given by $(2 - 1/q)^{1/4}$. The horizontal dashed-dotted line indicates the constant value $2^{1/4} \approx 1.19$.

effectively $\eta = 1 + 1/q$ more segments have to be analyzed (hence 50–100% more data).

In practice, the choice of q (or equivalently η) will generally have to be optimized in terms of search sensitivity at the given computational constraints and code implementation at hand, as well as for the detector data available. Further investigation in this direction will be presented in Sec. VI, comparing the estimated search sensitivity at fixed computational cost.

V. SENSITIVITY PERFORMANCE DEMONSTRATION

The performance improvement of the sliding coherence window technique is illustrated through realistic Monte Carlo simulations. In particular, receiver operating characteristic (ROC) curves are obtained to compare the standard hierarchical search scheme that is $q = 1$ (corresponding to $\eta = 0$) and the sliding coherence window strategy for $q = 2$ (corresponding to $\eta = 50\%$).

The simulated data set refers to the two LIGO 4-km detectors (H1 and L1) and spans a time interval of 5000 h. To provide a realistic comparison, a typical value is taken for the coherent time baseline of $T = 50$ h, which results in $N = 100$. The software tools used are part of LALAPPS [47] and employ accurate barycentering routines with timing errors below 4 μs [48].

In this study, the phase parameter space considered is four dimensional using one spindown parameter, as in current all-sky surveys for prior unknown CW sources [15–17]. Thus a point in phase parameter space is labeled by $\mathbf{p} = (f, \dot{f}, \alpha, \delta)$.

The false alarm probabilities are found from thousands of different realizations of stationary Gaussian white noise with $\sqrt{S_n} = 3.25 \times 10^{-22}$ Hz$^{-1/2}$. To obtain the detection probabilities, distinct CW signals with fixed gravitational-wave strain tensor amplitude of $h_0 = 1.0 \times 10^{-24}$ are added. The remaining parameters of the signal population are randomly drawn from uniform distributions in ψ, $\cos\iota$, Φ_0, in the entire sky, frequencies in the interval $f \in [155.12, 155.16]$ Hz, and spindowns over the range of $\dot{f} \in [-2.64, 0.264]$ nHz/s.

Figure 3 compares the resulting ROC curves for the different search techniques. The ROC curves are computed from 6000 different realizations. The 1σ errors shown in Fig. 3 are based on a jackknife estimate as in [49,50] using 100 subsets. As expected, the sliding coherence window technique with $q = 2$ is substantially more "powerful" than the standard scheme (retrieved for $q = 1$), yielding a higher probability of detection for the same false alarm probability.

Furthermore, the numerical results in Fig. 3 attest to the analytically estimated gain in sensitivity obtained in Eq. (51). For example, at fixed false alarm probability of $P_{\mathrm{FA}} = 1\%$, the achieved detection probability of the sliding coherence window technique is $P_{\mathrm{DET}} = 0.427$,
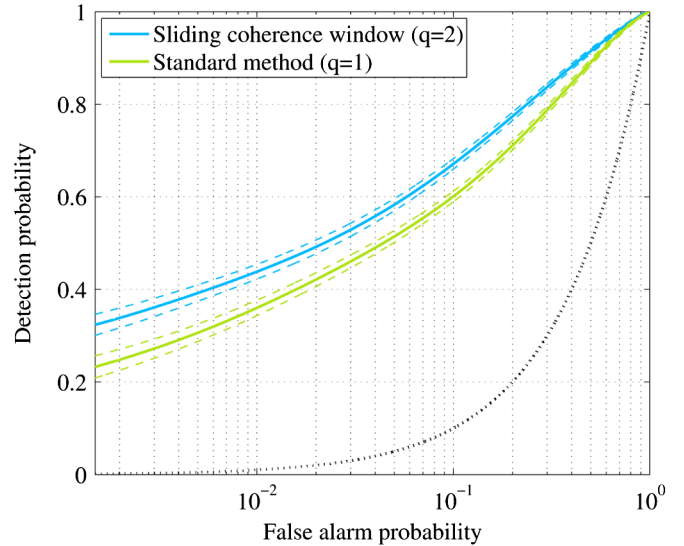

FIG. 3 (color online). ROC curves comparing at fixed gravitational-wave amplitude h_0 the standard hierarchical search technique (lower solid curve) and the sliding coherence window method (upper solid curve) with $q = 2$ implying a coherence overlap of $\eta = 50\%$. The dashed curves on either side of the solid curves represent estimated 1σ errors. The black dotted curve is the so-called line of no discrimination.

whereas the standard hierarchical scheme gives $P_{\mathrm{DET}} = 0.356$. To compare these values with the theoretical expectation, note that Eq. (51) yields $\sqrt{\mathcal{E}} \propto (2 - 1/q)^{1/4}$, where $\mathcal{E}$ has been defined in Eq. (48) and solely depends on P_{FA} and P_{DET}. Thus, for $q = 2$, the predicted increase (compared to $q = 1$) in $\sqrt{\mathcal{E}}$ is $(3/2)^{1/4} \approx 10.7\%$. The above values obtained from the numerical simulations of Fig. 3 yield a corresponding increase in $\sqrt{\mathcal{E}}$ of about 9.7%, which is in agreement with the theoretical prediction at the sub-percent level.

VI. COMPARISON AT FIXED COMPUTING COST

In Sec. IV B, Eq. (51) presented the sensitivity estimate of the sliding coherence window technique for a given (finite) amount of data, disregarding aspects of computational cost and essentially assuming unlimited computing power available. The present section investigates the contrary case, finding the amount of data which can be analyzed at limited (fixed) computational resources and a given (fixed) coherence time baseline T.

The computing cost $\zeta^{(1)}$ of a standard two-stage hierarchical search per a certain volume of phase parameter space searched can always be written as a sum in terms of implementation-specific constants ζ_{COH} and ζ_{INCOH} pertaining to the coherent and incoherent combination stage, respectively, as

$$\zeta^{(1)} = (\zeta_{\mathrm{COH}} + \zeta_{\mathrm{INCOH}} \gamma^{(1)}) N^{(1)}, \qquad (53)$$

where $\gamma^{(1)}$ denotes the so-called refinement factor [33] of the incoherent combination stage, and $N^{(1)}$ are the number of segments coherently analyzed.

The computational cost $\zeta^{(q)}$ of the sliding coherence window technique involves q times more summations at the incoherent combination stage, thus,

$$\zeta^{(q)} = (\zeta_{\text{COH}} + \zeta_{\text{INCOH}}\gamma^{(q)}q)N^{(q)}. \tag{54}$$

The total amount of data which can be analyzed at the fixed computational expense using the standard hierarchical search scheme is taken as $T_{\text{data}}^{(1)} = TN^{(1)}$. In analogy, the amount of data that can be searched at given computing cost using the sliding coherence window approach is $T_{\text{data}}^{(q)} = TN^{(q)}$, for the same coherent time baseline T.

The sensitivity of the standard hierarchical search scheme follows $h_0^{(1)} \propto (T_{\text{data}}^{(1)}T)^{-1/4}$. Accordingly, the sensitivity of the sliding coherence window technique given in Eq. (51) scales as $h_0^{(q)} \propto (T_{\text{data}}^{(q)}T)^{-1/4}(2 - 1/q)^{-1/4}$. Thus, we define the sensitivity ratio by $r \equiv h_0^{(1)}/h_0^{(q)}$, which takes the form

$$r = \left(\frac{T_{\text{data}}^{(q)}}{T_{\text{data}}^{(1)}}\right)^{1/4}\left(2 - \frac{1}{q}\right)^{1/4}. \tag{55}$$

At equal total computing cost, $\zeta^{(q)} = \zeta^{(1)} = \zeta$, inverting Eqs. (53) and (54) for $T_{\text{data}}^{(1)}$ and $T_{\text{data}}^{(q)}$, respectively, one obtains

$$r = \left(\frac{2}{q} - \frac{1}{q^2}\right)^{1/4}\left(\frac{\sqrt{1 + 4q\theta} - 1}{\sqrt{1 + 4\theta} - 1}\right)^{1/4}, \tag{56}$$

where the constant θ has been defined as

$$\theta \equiv \frac{\zeta\zeta_{\text{INCOH}}}{\zeta_{\text{COH}}^2}, \tag{57}$$

and the refinement factors have been approximated by $\gamma^{(q)} \approx N^{(q)}$, assuming the search includes at most one spindown parameter (cf. Ref. [33]).

Figure 4 illustrates the sensitivity ratio r of Eq. (56) as a function of θ and for different values of q. Two regimes are identified where r is slowly changing: when θ is either very small or very large. This can be understood as follows. The specific value of θ depends on the code implementation, manifested in the two constants ζ_{COH} and ζ_{INCOH}. Thus, in the two extreme cases where one constant is much larger than the other, the two different limits of r result.

First, if the implementation is such that the coherent part dominates the computing cost ($\zeta_{\text{COH}} \gg \zeta_{\text{INCOH}}$), this implies that θ is very small. Then the sensitivity ratio is described by

$$\lim_{\theta \to 0} r = \left(2 - \frac{1}{q}\right)^{1/4} = (1 + \eta)^{1/4}, \tag{58}$$

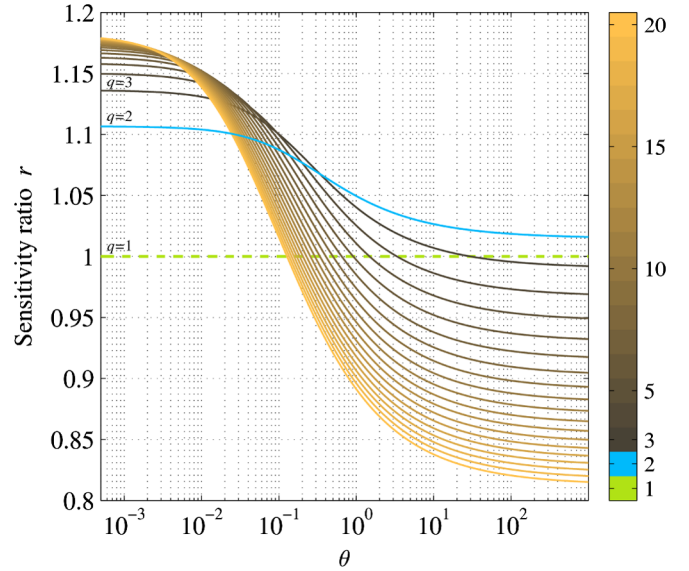which is the same improvement factor as given by Eq. (52).

FIG. 4 (color online). Estimated sensitivity ratio r as introduced in Eq. (57) of the standard hierarchical search and the sliding coherence window technique at fixed total computational cost and given T, shown as a function of θ defined in Eq. (57). The different curves correspond to different values of q (number of subsegments) as indicated by the shaded [color] bar. The dashed horizontal line corresponds to $q = 1$, for which the search methods coincide.

On the other hand, if the incoherent part is the most computationally intensive ($\zeta_{\text{INCOH}} \gg \zeta_{\text{COH}}$), θ takes a very large value. In this case, the sensitivity ratio is described by

$$\lim_{\theta \to \infty} r = \left(2 - \frac{1}{q}\right)^{1/4}q^{-1/8}. \tag{59}$$

It is interesting to note that, only for $q = 2$, the sensitivity ratio is *always* greater than 1, implying that in this case the sliding coherence window technique should always be more sensitive than the standard scheme at given T and fixed computational cost.

In the current EINSTEIN@HOME [18] analysis, θ is approximately of order 10^{-2}. Thus, the situation in this case is rather comparable to the regime described by Eq. (58). Hence, the EINSTEIN@HOME search sensitivity will certainly benefit from employing the sliding coherence window technique.

VII. CONCLUSION

In summary, a novel hierarchical strategy to search for prior unknown continuous gravitational-wave sources has been presented, exploiting a sliding coherence window. The standard hierarchical search scheme divides the data into N nonoverlapping segments that are coherently analyzed, and subsequently matched-filter outputs are combined incoherently. Thereby, the duration of one segment defines the maximum time span of coherence. In contrast, the presented sliding coherence window approach divides

each of the N data segments into q subsegments, which are thus *shorter* than the desired maximum coherence length T (size of the coherence window). This permits the efficient combination of matched-filter outputs from all subsegments in a ''sliding-window'' fashion: If subsegments are closer than T, they are combined coherently; otherwise, they are combined incoherently.

As a result, the estimated search sensitivity of the sliding coherence window approach is considerably superior compared to the standard hierarchical scheme, while using the *same* number of coarse- and fine-grid templates to cover the search parameter space. At a given value of T, the sensitivity improvement in terms of minimum detectable gravitational-wave amplitude h_0 scales with the fourth root of $N(2 - 1/q)$ for a contiguous data set. Since for the standard hierarchical method $q = 1$, to achieve the same sensitivity as the sliding coherence window technique between 50–100% more data (to increase N accordingly) would have to be analyzed. Realistic Monte-Carlo simulations have been carried out confirming the sensitivity enhancement.

The sensitivity improvement can also be expressed in terms of the average coherence overlap η between successive sliding steps. In particular, if the data set has gaps in time, η can be a useful figure of merit. The estimated sensitivity improvement of the sliding coherence window technique over the standard scheme scales as the fourth root of $(1 + \eta)$.

In addition, the sensitivity has also been compared at fixed computational cost. When the computing cost of the coherent stage dominates, the above sensitivity improvement holds. In the case where the computational cost of the incoherent stage dominates, the sensitivity improvement can fade away, depending on the search

setup. However, it is estimated that, when the chosen coherence window is equal to the length of 2 subsegments, the sensitivity is always superior to the standard method at about the same computational expense. In general, the search setup (including the choice of q) will have to be sensitivity optimized at the given computational resources and the software at hand, as well as for the data available.

However, further topics are planned to be investigated in future work. One of these aspects concerns the efficient implementation of the proposed technique while exploiting the FFT algorithm. Moreover, an optimal weighting scheme between the coherent matched-filter outputs from different subsegments could be further studied, taking into account correlations between these.

The sliding coherence window approach is envisioned to be employed by the EINSTEIN@HOME [18] project to further improve the search sensitivity of all-sky surveys for unknown isolated CW sources [26]. The proposed approach should also be extensible to CW searches for sources in binary systems [51]. With suitable modification, the method might also have applicability in further related areas, for instance, regarding computationally limited searches for prior unknown radio [52], X-ray [53], and gamma-ray pulsars [54–57].

ACKNOWLEDGMENTS

[1] B. J. Owen, L. Lindblom, C. Cutler, B. F. Schutz, A. Vecchio, and N. Andersson, Phys. Rev. D **58**, 084020 (1998).

[2] G. Ushomirsky, C. Cutler, and L. Bildsten, Mon. Not. R. Astron. Soc. **319**, 902 (2002).

[3] C. Cutler, Phys. Rev. D **66**, 084025 (2002).

[4] D. I. Jones and N. Andersson, Mon. Not. R. Astron. Soc. **331**, 203 (2002).

[5] B. J. Owen, Phys. Rev. Lett. **95**, 211101 (2005).

[6] C. J. Horowitz and K. Kadau, Phys. Rev. Lett. **102**, 191102 (2009).

[7] *Neutron Stars and Pulsars*, edited by W. Becker (Springer, Berlin, Heidelberg, 2009).

[8] B. Abbott *et al.* (LIGO Scientific Collaboration), Rep. Prog. Phys. **72**, 076901 (2009).

[9] F. Acernese *et al.* (Virgo Scientific Collaboration), Classical Quantum Gravity **23**, S635 (2006).

[10] H. Grote *et al.* (LIGO Scientific Collaboration), Classical Quantum Gravity **25**, 114043 (2008).

[11] R. Takahashi *et al.* (TAMA Collaboration), Classical Quantum Gravity **21**, S403 (2004).

[12] B. Abbott *et al.* (LIGO Scientific Collaboration), Astrophys. J. Lett. **683**, L45 (2008).

[13] B. Abbott *et al.* (LIGO Scientific Collaboration), Astrophys. J. **713**, 671 (2010).

[14] B. Abbott *et al.* (LIGO Scientific Collaboration), Phys. Rev. D **77**, 022001 (2008).

[15] B. Abbott *et al.* (LIGO Scientific Collaboration), Phys. Rev. Lett. **102**, 111102 (2009).

[16] B. Abbott *et al.* (LIGO Scientific Collaboration), Phys. Rev. D **79**, 022001 (2009).

[17] B. Abbott *et al.* (LIGO Scientific Collaboration), Phys. Rev. D **80**, 042003 (2009).

[18] EINSTEIN@HOME is available at http://einstein.phys.uwm.edu/.

[19] N. Andersson, V. Ferrari, D. I. Jones, K. D. Kokkotas, B. Krishnan, J. S. Read, L. Rezzolla, and B. Zink, Gen. Relativ. Gravit. **43,** 409 (2010).

[20] P. Jaranowski, A. Królak, and B. F. Schutz, Phys. Rev. D **58,** 063001 (1998).

[21] C. Cutler and B. F. Schutz, Phys. Rev. D **72,** 063006 (2005).

[22] P. R. Brady, T. Creighton, C. Cutler, and B. F. Schutz, Phys. Rev. D **57,** 2101 (1998).

[23] P. Patel, X. Siemens, R. Dupuis, and J. Betzwieser, Phys. Rev. D **81,** 084032 (2010).

[24] C. Cutler, I. Gholami, and B. Krishnan, Phys. Rev. D **72,** 042004 (2005).

[25] B. Krishnan, A. M. Sintes, M. A. Papa, B. F. Schutz, S. Frasca, and C. Palomba, Phys. Rev. D **70,** 082001 (2004).

[26] H. J. Pletsch and B. Allen, Phys. Rev. Lett. **103,** 181102 (2009).

[27] H. J. Pletsch, Phys. Rev. D **78,** 102005 (2008).

[28] R. Prix and Y. Itoh, Classical Quantum Gravity **22,** S1003 (2005).

[29] R. Balasubramanian, B. S. Sathyaprakash, and S. V. Dhurandhar, Phys. Rev. D **53,** 3033 (1996).

[30] B. J. Owen, Phys. Rev. D **53,** 6749 (1996).

[31] I. Jones, B. J. Owen, and D. Whitbeck, LIGO Document No. T0900500-v1, 2005, available at https://dcc.ligo.org/.

[32] R. Prix, Phys. Rev. D **75,** 023004 (2007).

[33] H. J. Pletsch, Phys. Rev. D **82,** 042002 (2010).

[34] P. Jaranowski and A. Królak, Phys. Rev. D **59,** 063003 (1999).

[35] P. Jaranowski and A. Królak, Phys. Rev. D **61,** 062001 (2000).

[36] Over the typical long coherent integration times of hierarchical CW searches as considered here, the Gaussian noise assumption can also be well justified in practice based on the central limit theorem for the vast majority of frequency bands of the real detector output (cf. the LIGO searches in [16,17]). There is also evidence [37] that the performance of the matched-filtering method for Gaussian noise is also satisfactory for the case of non-Gaussian noise.

[37] L. S. Finn, Phys. Rev. D **63,** 102001 (2001).

[38] R. Prix and J. T. Whelan, Classical Quantum Gravity **24,** S565 (2007).

[39] J. T. Whelan, R. Prix, and D. Khurana, Classical Quantum Gravity **25,** 184029 (2008).

[40] J. T. Whelan, R. Prix, and D. Khurana, Classical Quantum Gravity **27,** 055010 (2010).

[41] One may further illustrate this by noting that the semicoherent metric is effectively the average of all individual-segment coherent metrics [26,33,42]. Thus, in this sense, at fixed coherence baseline T and at fixed total data time span T_{data}, the additional overlapping segments do not change the averaged metric [43].

[42] P. R. Brady and T. Creighton, Phys. Rev. D **61,** 082001 (2000).

[43] B. Krishnan (private communication).

[44] Equivalently, one could also employ the pairs $\{\hat{\mathcal{A}}_\mu^{[k]}, \hat{\mathcal{A}}_\nu^{[\ell]}\}$.

[45] The covariance matrix of the Gaussian random variables $x_\mu^{[k]}$ can always be diagonalized via a linear transformation given by Eq. (65) of Ref. [20]. Besides, C_k exactly vanishes when computed over a time interval of a multiple of one sidereal day [35]. Also note that, when averaged over all sky positions (α, δ), in contrast to A_k and B_k, the constant C_k vanishes.

[46] When the data contains gaps, the average coherence overlap η is a function of the subsegment time midpoints t_k.

[47] http://www.lsc-group.phys.uwm.edu/daswg/.

[48] B. Abbott et al., Phys. Rev. D **69,** 082004 (2004).

[49] R. Prix and B. Krishnan, Classical Quantum Gravity **26,** 204013 (2009).

[50] J. H. Conway and N. J. A. Sloane, SIAM J. Algebr. Discrete Methods **5,** 294 (1984).

[51] C. Messenger, LIGO Document P1000020-v1, 2010, available at https://dcc.ligo.org/.

[52] S. M. Ransom, S. S. Eikenberry, and J. Middleditch, Astron. J. **124,** 1788 (2002).

[53] B. A. Vaughan et al., Astrophys. J. **435,** 362 (1994).

[54] A. M. Chandler, D. T. Koh, R. C. Lamb, D. J. Macomb, J. R. Mattox, T. A. Prince, and P. S. Ray, Astrophys. J. **556,** 59 (2001).

[55] W. B. Atwood, M. Ziegler, R. P. Johnson, and B. M. Baughman, Astrophys. J. Lett. **652,** L49 (2006).

[56] A. A. Abdo et al., Science **325,** 840 (2009).

[57] P. M. Saz Parkinson et al., Astrophys. J. **725,** 571 (2010).